

Under-ice acoustic navigation using real-time model-aided range estimation

EeShan C. Bhatt,^{1, 2, a} Oscar Viquez,² and Henrik Schmidt²

¹*MIT-WHOI Joint Program in Oceanography/Applied Ocean Science & Engineering,
Cambridge and Woods Hole, MA, USA*

²*Department of Mechanical Engineering, Massachusetts Institute of Technology,
Cambridge, MA*

(Dated: 21 February 2022)

1 The long baseline (LBL) underwater navigation paradigm relies on the conversion
2 of recorded travel times into pseudoranges to trilaterate position. For real-time op-
3 erations, this conversion has assumed an isovelocity sound speed. For re-navigation
4 in post-processing, computationally and/or labor intensive acoustic modeling may
5 be employed to reduce uncertainty driven by multipath arrivals. This work demon-
6 strates a real-time ray-based prediction method of the effective sound speed along
7 a path from source to receiver to minimize vehicle position error. This method was
8 implemented for a small scale AUV-LBL system in March 2020, in the Beaufort Sea,
9 in total ice-covered conditions and a double ducted acoustic propagation environ-
10 ment. The vehicle was successfully deployed and recovered. Given the lack of GPS
11 data throughout the vehicle’s mission, however, the pseudorange performance is first
12 evaluated on connections between GPS-linked beacons. The real-time ranging error
13 between beacons is roughly 11 meters at distances up to 3 km. But a consistent over-
14 estimation in the real-time method provides insights for improved eigenray filtering
15 by the number of surface bounces. An operationally equivalent pipeline is used to
16 re-position the LBL beacons and re-navigate the AUV, using a modeled, historical,
17 and a locally observed sound speed profile. The median re-navigation error is 1.84 ± 2.19 RMS m. The improved trilateration performance for suggests that this ap-
18 proach effectively extends the single meter accuracy of the deployed GNSS units into
19 the water column.

^aebhatt@whoi.edu

²¹ **I. INTRODUCTION**

²² Autonomous underwater vehicles (AUVs) are increasingly capable platforms to explore
²³ and sample the ocean, particularly for remote and/or dangerous regions. However, navi-
²⁴ gation uncertainty is a major challenge in considering AUVs as standard tools for oceano-
²⁵ graphic research. While land and air-based robots utilize information from Global Naviga-
²⁶ tion Satellite Systems (GNSS) to achieve stunning location accuracy and precision through-
²⁷ out the duration of their missions, AUVs cannot access GNSS fixes while underwater. There-
²⁸ fore, underwater vehicles have relied on any combination of dead reckoning, hydrodynamic
²⁹ models, inertial navigation systems, doppler velocity logs, and acoustic baseline positioning
³⁰ systems for navigation (Paull *et al.*, 2014). Limiting navigation error and drift requires an
³¹ AUV to periodically stall on the surface and obtain a GNSS fix to reset its position error.
³² This foolproof method of self-positioning is undesirable for stealth, adverse weather condi-
³³ tions, and mission efficiency, and inaccessible in a GNSS-denied situation like an ice-covered
³⁴ environment.

³⁵ Of underwater acoustic navigation systems, long baseline (LBL) is the most GPS-like
³⁶ in style and scale, and most appropriate for mitigating drift without overburdening com-
³⁷ putation or payload size on the vehicle (Van Uffelen, 2021). The state-of-the-art for LBL
³⁸ outsources depth to a pressure sensor and solves the two-dimensional localization problem
³⁹ with an isovelocity, linear scaling between one way travel time (OWTT) and range (Eustice
⁴⁰ *et al.*, 2006, 2007; Webster *et al.*, 2009, 2012). This assumption is valid for short scale
⁴¹ operations but oversimplifies propagation for larger and/or complex acoustic environments.

42 To achieve single meter, GNSS-like performance in a GNSS-denied environment, we demon-
 43 strate an embedded ray-based data processing algorithm to convert recorded OWTTs into
 44 pseudorange estimates. This methodology was integrated onto the AUV *Macrura*, deployed
 45 and recovered in the Beaufort Sea, in March 2020, during the Ice Exercise 2020 (ICEX20).
 46 A physics-driven methodology that received an *in situ* sound speed profile (SSP) was nec-
 47 essary despite the small operational domain because of the relatively high-risk mission en-
 48 vironment—total under-ice conditions and a variable double ducted acoustic environment.
 49 For consistency, we delineate specific definitions for timing, positioning, and navigation
 50 from [Howe et al. \(2019\)](#).

- 51 1. Timing is the ability to acquire and maintain accurate and precise time anywhere in
 52 the domain of interest within user-defined timeliness parameters
- 53 2. Positioning is the ability to accurately and precisely determine one's location refer-
 54 enced to a standard geodetic system
- 55 3. Navigation is the ability to determine current and desired position (relative or absolute)
 56 and apply corrections to course, orientation, and speed to attain a desired position
 57 anywhere in the domain of concern

58 Thus, navigation is inherently in real-time and depends on positioning; positioning depends
 59 on timing. We also suggest re-navigation and re-positioning as post-processed corollaries,
 60 which may include knowledge or processing capabilities not available *in situ*.

61 While RAFOS floats championed one way ranging for re-positioning ([Duda et al., 2006](#);
 62 [Rossby et al., 1986](#)), the ability to do so for navigation was facilitated by the advent of

the WHOI Micro-Modem (Singh *et al.*, 2006) and synchronized clocks (Rypkema *et al.*, 2017). AUV navigation efforts have achieved root mean square (RMS) localization error on the order of tens of meters relative to GNSS surface position over less than ten kilometers in shallow (Claus *et al.*, 2018; Eustice *et al.*, 2007; Kepper *et al.*, 2017) and deep water (Jakuba *et al.*, 2008; Kunz *et al.*, 2008; Webster *et al.*, 2009). However, these efforts all used a nominal sound speed for travel time conversion and the vehicles were limited to shallower isovelocity regimes.

Localization algorithms that do consider environmental or acoustic uncertainty tend to focus on longer and larger experiments, where spatio-temporal variability cannot be ignored. These methods have also been reserved for post-processing as they can be labor intensive, computationally heavy, and/or require additional information like contemporaneous data. For example, gliders navigating with kinematic flight models and equipped with acoustic modems were later unambiguously associated with predicted ray arrivals, resulting in roughly a kilometer error and hundred meters uncertainty over basin scale propagation (Van Uffelen *et al.*, 2013). A follow up study investigated how a single temporally and spatially averaged SSP could mitigate position error for a four month glider mission (Uffelen *et al.*, 2016). Wu *et al.* (2019) cross correlate three days of real acoustic records with synthetic ones generated through ocean model snapshots from HYCOM (Chassagnet *et al.*, 2007). While potentially applicable for various ocean states, this is reliant on model realism and impractical for real-time operations. Mikhalevsky *et al.* (2020) introduces a “cold start” algorithm that does not require prior knowledge of track, position, or sound speed information. The algorithm inputs a four-dimensional ocean model, constrained by tomography data, into a range dependent

85 ray code to isolate the last path detected in a full multipath pattern. Then, a representative
86 group speed is solved for alongside position in a least squares fashion. This approach is able
87 to re-position a floating hydrophone array with an error of 58 m and a standard deviation
88 of 32 m based on six sources 129–450 km away but remains to seen for real-time navigation.

89 The ICEX20 AUV deployment necessitated an environmentally- and physically-driven
90 relationship between recorded travel times and estimated pseudoranges due to the multipath
91 uncertainty brought upon by an increasingly observed double ducted environment in the
92 Beaufort Sea, which some refer to as the “Beaufort Lens” (Chen *et al.*, 2019; Chen and
93 Schmidt, 2020; Litvak, 2015).

94 Given that a lens introduces significant ray refraction, the Beaufort Lens is a shorthand for
95 the spatio-temporal variability of the local temperature and sound speed maxima generally
96 around 50 to 60 m in depth. A neutrally buoyant layer of warm Pacific Summer Water
97 creates a unique double ducted environment —the upper duct degrades signal coherence
98 due to intensified ice interaction and the lower duct effectively traps sound for long range
99 propagation (Poulsen and Schmidt, 2017). Modeling output (Duda *et al.*, 2021, 2019) and
100 experimental observations (Ballard *et al.*, 2020; Bhatt, 2021) suggest that, in the Beaufort
101 Sea, the duct is persistent and widespread but not necessarily continuous; it and its acoustic
102 effects can be non-existent, minimal, or drastic. Transmissions in the upper duct, between
103 the surface ice and the lens, experience minimal attenuation but degrade in signal coherence
104 with repeated reflections under the ice. In lower duct, between the lens and its conjugate
105 depth in the Atlantic water, roughly 200 m, sound above 350 Hz is trapped near losslessly
106 for long range propagation (Poulsen and Schmidt, 2017).

107 The Arctic, while remote, is the perfect place to demonstrate mature navigation tech-
 108 nologies in real GNSS-denied conditions. Thorough reviews of uncrewed vehicle operations
 109 in polar environments can be found in (Norgren *et al.*, 2014) and (Barker *et al.*, 2020); there
 110 is no comparable work in the Arctic for a short range AUV deployment in the Beaufort
 111 Lens. Seminal (Bellingham *et al.*, 1995; Brooke, 1981; Hayes and Morison, 2002; Jackson,
 112 1983; Light and Morison, 1989) and more recent AUV deployments (Fossum *et al.*, 2021;
 113 Jakuba *et al.*, 2008; Kukulya *et al.*, 2010; Kunz *et al.*, 2008; Plueddemann *et al.*, 2012; Tim-
 114 mermans and Winsor, 2013) witnessed the classical upward refracting sound speed profile
 115 that is amenable to an isovelocity assumption.

116 Of note, despite different platforms and scales, are recent glider deployments in the
 117 Canada Basin. In 2014, in partially ice-covered conditions, a long range LBL system with
 118 WHOI Micro-Modems at 100 m exploited the lower duct for long range communication with
 119 two gliders (Freitag *et al.*, 2016; Webster *et al.*, 2015). The sound speed value measured at
 120 the time of reception was used to estimate pseudorange in post-processing. The beacon-to-
 121 beacon performance was excellent, achieving contact at ranges greater than 200 km with
 122 a position uncertainty of 40 m. The beacon-to-glider performance, however, deteriorated
 123 due to missed contacts outside the duct, and was not described quantitatively. In 2017,
 124 gliders were deployed in a region with no ice coverage (Graupe *et al.*, 2019). Ranges were
 125 linearly scaled by a statistical description of sound speed observations taken during the
 126 experiment, 1450 ± 6.5 m/s. This resulted in an error of 550 m, which was reduced by
 127 a factor between 4 and 5, depending on the dive, using a post-processing acoustic arrival
 128 matching method. Both cases exploit the lower duct for high fidelity communication at

¹²⁹ long ranges. Unintuitively, the smaller nature of our deployment during ICEX20 is not a
¹³⁰ simplifying factor. For source depths typical to vehicle operations, 30 to 200 m, a shadow
¹³¹ zone spans from 2 to 6 kilometers in range ([Schmidt and Schneider, 2016](#)).

¹³² Compared to the previous small scale navigation efforts, the approach in this paper
¹³³ integrates real-time model-aided data processing to estimate a representative sound speed
¹³⁴ along a path from source to receiver, leveraging climatology, *in situ* data, and fast acoustic
¹³⁵ modeling. The paper is organized as follows. Section [II](#) details the experimental approach
¹³⁶ and conditions during ICEX20. Given that there is no GNSS ground truth for the vehicle
¹³⁷ position while underway, we first evaluate the real-time ranging performance of GPS-linked
¹³⁸ beacon-to-beacon communication events in section [III](#). Section [IV](#) uses insights from field
¹³⁹ data to introduce a new ray filtering algorithm to improve range estimation. Section [V](#)
¹⁴⁰ emulates the real-time processing pipeline to re-position beacon-to-beacon events and re-
¹⁴¹ navigate AUV *Macrura*.

¹⁴² **II. OVERVIEW OF THE ICEX20 EXPERIMENT**

¹⁴³ The results from this paper derive from data taken while deploying the AUV *Macrura*, a
¹⁴⁴ custom Bluefin-21, during the Ice Exercise 2020 (ICEX20), in the Beaufort Sea, from March
¹⁴⁵ 8th to 11th. The AUV deployment was supported by the Integrated Communication and
¹⁴⁶ Navigation Network (ICNN) ([Randeni et al., 2020, 2021; Schneider et al., 2020](#)), a special-
¹⁴⁷ ized implementation of the LBL solution. The ICNN was initially developed via numerous
¹⁴⁸ virtual experiments to ensure robust algorithms and interfaces between different hardware
¹⁴⁹ components. The simulation capabilities are largely physics-driven with a modular system of
¹⁵⁰ systems approach—an environmental simulator with sub-components for the ocean, includ-
¹⁵¹ ing Arctic ice drift and ocean acoustic propagation; a vehicle simulator with sub-components
¹⁵² for vehicle dynamics and navigation; a topside hardware simulator and acoustic communica-
¹⁵³ tions simulator, both with a software-only configuration and a hardware-in-the-loop version
¹⁵⁴ ([Schneider and Schmidt, 2018](#)). The virtual environment similarly emulates the interfaces
¹⁵⁵ between the real components to test the entire software pipeline.

¹⁵⁶ **A. The Integrated Communication and Navigation Network**

¹⁵⁷ The ICNN is comprised of four ice buoys in a loose rectangle, roughly 2 km away from
¹⁵⁸ a central ice camp with a topside computer, as shown in Fig. 1. Each ice buoy is outfitted
¹⁵⁹ with a Garmin GPS 18x, with a pulse-per-second rising edge aligned to 1 microsecond and
¹⁶⁰ a spec sheet accuracy of 3 m, 95% of the time. The AUV and each ice buoy are outfitted
¹⁶¹ with a WHOI Micro-Modem ([Singh et al., 2006](#)), with a four-element receiver array, a single

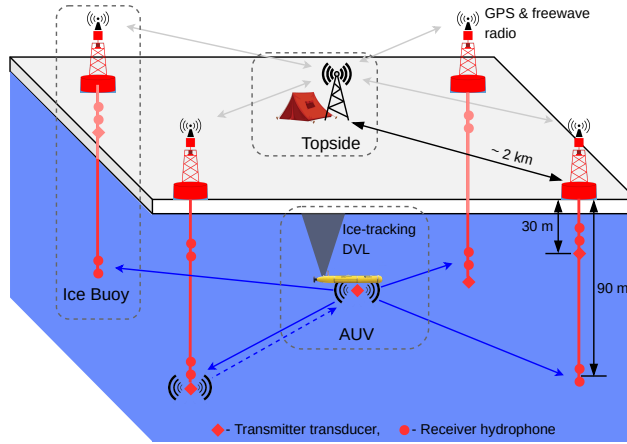


FIG. 1. A schematic overview of the Integrated Communication and Navigation Network (ICNN), which provides joint data-transfer and tracking between AUV and a human decision maker at Topside.

162 transmitter, and one-tenth of a millisecond resolution. Acoustic messages were sent with
 163 a 10 kHz carrier frequency, 5 kHz bandwidth, and phase-shift keying (PSK) modulation on
 164 a time-division multiple access schedule with a thirty-second cycle, giving room for two-
 165 way communication throughout the mission volume. The receive and transmit elements
 166 were split between shallow and deeper depths—30 and 90 m—to provide better coverage
 167 across the shadow zone. While each buoy only has one transmit depth, all buoys have both
 168 receive depths but the active receive layer is consistent across all buoys. The design of
 169 the ICNN enables a self-adapting network to transmit and receive at the optimal depth to
 170 maintain contact with the AUV ([Schneider et al., 2020](#)). The buoys do not encompass the
 171 full horizontal range of the vehicle but are positioned to minimize overlap in trilateration
 172 for spherical positioning ([Deffenbaugh et al., 1996a](#)).

173 To balance competing uses of the acoustic channel, the network uses a single synchronized

174 digital communication packet to provide both tracking and data to the operator.

175 1. The AUV, running an ice-tracking DVL and an onboard hydrodynamic model, broad-

176 casts its perceived location on a scheduled, time-synchronized message via WHOI

177 Micro-Modem

178 2. Four ice buoys, each outfitted with a WHOI Micro-Modem, receive messages from the

179 AUV and send that information over freewave radio to a Topside computer

180 3. The topside computer converts travel times into pseudorange estimates using a stochas-

181 tic embedded prediction of the horizontal group velocity via BELLHOP ray tracing

182 code ([Porter, 2011](#)) using a sound speed profile provided by an updatable Virtual

183 Ocean ([Bhatt et al., 2022; Schneider and Schmidt, 2018](#))

184 4. The topside computer calculates a new position by trilaterating the range estimates

185 5. The position differential, not the absolute position, is broadcast to the vehicle to

186 update its navigation solution and be robust to latency and intermittency

187 In the face of GNSS-denied navigation, this approach was anecdotally successful, as shown

188 in Fig. 2. The AUV *Macrura* was deployed through a hydrohole from an ice camp but re-

189 covered through an emergency hydrohole. A random disk error stalled *Macrura* underneath

190 the ice but did not prevent it from transmitting its location. Due to an incoming storm, a

191 team placed a physical marker on the ice at the location. Three days later, *Macrura* was

192 found within a meter of the marker. We view the emergency recovery as qualitative proof

193 of the robustness of this navigation approach. Nonetheless, this paper specifically addresses

194 the third and fourth steps—the conversion of travel times into pseudoranges and its effect
 195 on trilateration. By focusing on pseudorange estimates between GPS-tracked beacons, and
 196 re-running the trilateration pipeline, the results are decoupled from all other mechanisms in
 197 the ICNN.

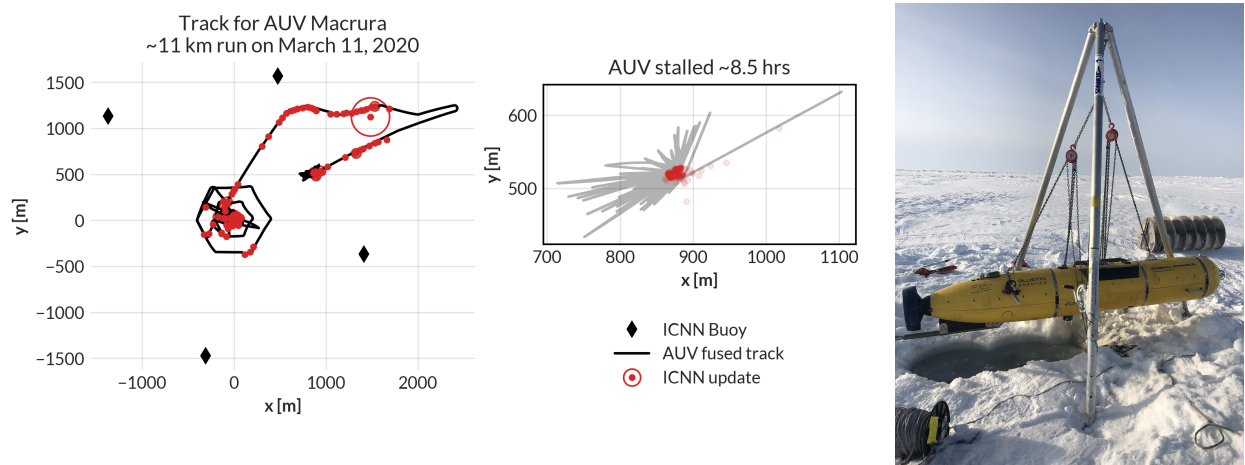


FIG. 2. The under-ice mission track for AUV *Macrura*, including the position updates as it stalled underneath the ice overnight. A marker was placed on the ice at the vehicle’s estimated self-location. It was recovered after a three day storm within a meter of the marker.

198 **B. ICEX20 sound speed conditions**

199 An important component to our navigation solution is an accurate estimation of a repre-
 200 sentative SSP for the ocean volume. Previous field experience, during the Ice Exercise 2016
 201 (ICEX16), demonstrated the negative effects of the Beaufort Lens on tracking and commu-
 202 nication (Schmidt and Schneider, 2016). Fig. 3 shows historical, modeled, and *in situ* sound
 203 speed data for both ICEX16 and ICEX20. These three input streams were selected to mirror

the information available on a submarine (personal conversation with LT B. Howard and LT CDR D. Goodwin). In the field, the SSP information was shared with the vehicle via basis representation compression on a lightweight digital acoustic message (Bhatt *et al.*, 2022). All modeled data comes from HYCOM (Chassignet *et al.*, 2007), which does not seem to capture the forcing mechanisms that cause the Beaufort Lens. For ICEX16, the data-driven profile was sourced from nearby Ice Tethered Profilers (ITP) after the field experiment (Krishfield *et al.*, 2008; Toole *et al.*, 2011) and exhibits a fairly low lens; the historical profile is from the World Ocean Atlas. For ICEX20, the chosen weights (data-driven) profile derives from an estimate of initial CTD casts taken on site, showing an intense warm water intrusion; the baseline (historical) profile, showing moderate ducted conditions, comes from the average of March 2013 ITP data. This month best matched sea ice and sound speed conditions at the beginning of ICEX20 (Bhatt *et al.*, 2022). It is important to note that all profiles that do show the Beaufort Lens do so with different local sound speed maxima at different depths, reflective of the wide range of lens properties observed for all ITP data in the region. The variability of the lens height and prominence is the main reason an updatable SSP was integrated into the ICNN solution.

During ICEX20, the HYCOM profile was available but never deployed. For post-processing comparison, we introduce both the HYCOM profile and an isovelocity case, 1441.8 ± 3.7 m/s, as the mean and standard deviation of the observed sound speed profile over the first 200 m. This is a contrived value taken in the style of Graupe *et al.* (2019) for the sake of comparison; the default value in the LAMSS simulator, which was not environmentally informed nor used during ICEX20, was 1430 m/s.

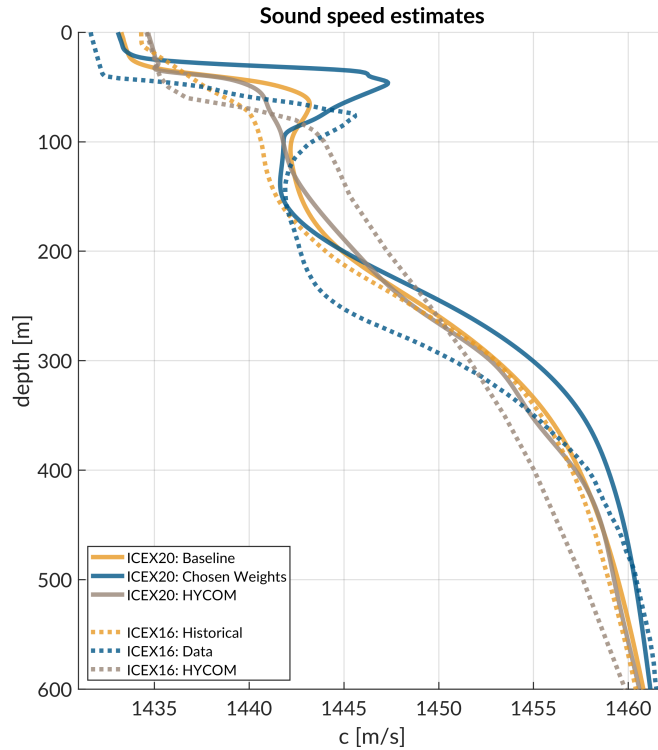


FIG. 3. Sound speed conditions for historical (baseline), data (chosen weights), and HYCOM model for both ICEX16 and ICEX20.

226 **III. REAL-TIME PSEUDORANGE ANALYSIS**

227 Because the vehicle’s navigation solution during a mission can only be evaluated on the
228 basis of the error estimates sent, a sister experiment for validating the real-time ranging
229 approach was implemented. Ice buoy modems were run as “virtual vehicles” at a fixed
230 depth, receiving position updates from the other beacons as well as a camp site modem
231 lowered to 20 m. Fig. 4 shows successful events sorted by source depth. In this analysis, we
232 assume there is insignificant displacement between the GNSS puck surface expression and
233 subsurface modem; this is supported by unusually low observed ice drift rates, just 0.7 cm/s
234 on average throughout the mission.

235 **A. Minimal bounce criteria (MBC)**

236 The fundamental challenge to implement GNSS-like navigation, especially in an acousti-
237 cally complex propagation environment, is characterizing a single sound speed to compensate
238 for the effects of ray refraction and reflection. The use of the acoustic modem network for
239 tracking relies on the accurate estimates of travel times between the submerged platform
240 and LBL beacons, supported by clock synchronization and a pre-determined scheduling of
241 acoustic events. For the Beaufort Lens in particular, the strong multipath effects make it
242 virtually impossible to deterministically predict the modem’s detected arrival time.

243 Instead, for each individual modem i , an embedded stochastic tracking framework is used
244 to provide a running estimate of the effective sound speed $c_{i,j}$ for the conversion from travel
245 time to range from modem j , with the ultimate goal of matching the implied horizontal

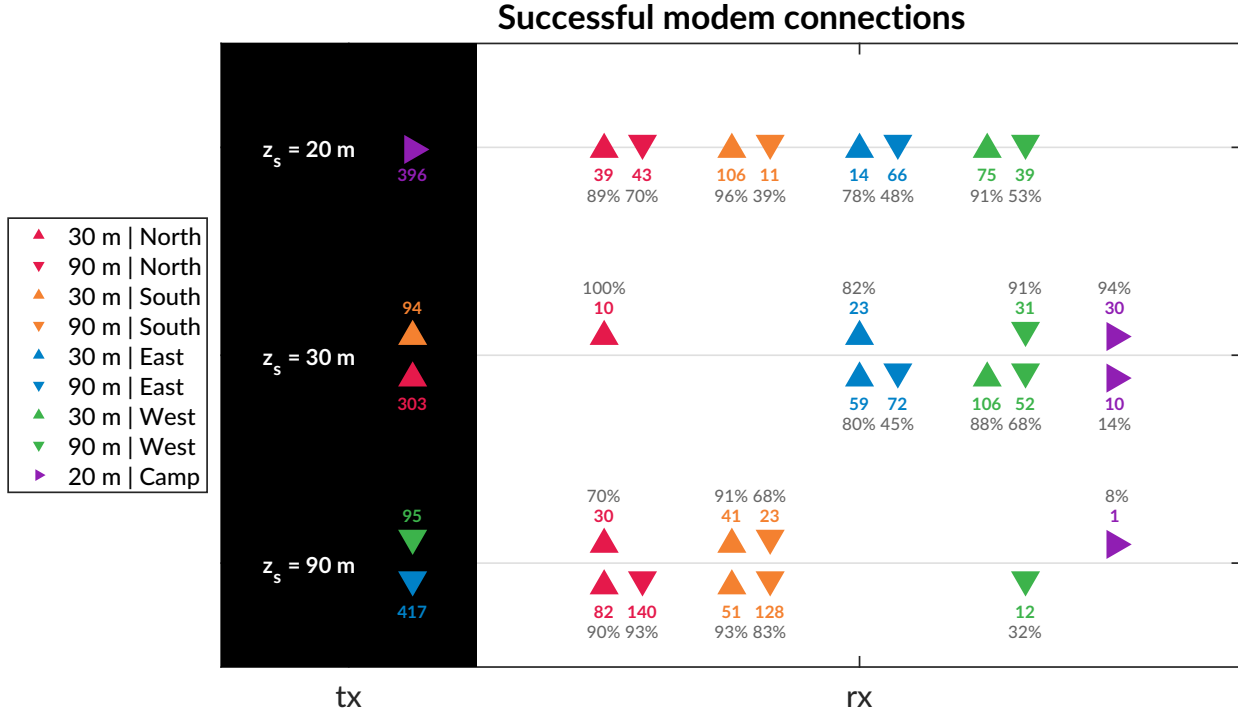


FIG. 4. An overview of the modem experiment by source and receiver depth and position. The black column on the left, *tx*, shows the source depth, z_s , with the total number of transmissions. The column on the right, *rx*, shows the receivers with the number of successful decodings and the percent success rate, defined as the ratio of decoded to detected. The orientation of the triangles—sideways, upwards, and downwards—corresponds to depths of 20, 30, and 90 m.

²⁴⁶ effective sound speed, i.e., the GPS-recorded distance between two nodes divided by the
²⁴⁷ modem-recorded one way travel time between them.

²⁴⁸ In the ICEX20 configuration, the acoustic tracking is running on the topside computer,
²⁴⁹ which controls the ICNN. Here we assume that the effective sound speeds $c_{i,j}$ are smoothly

250 varying over the course of a vehicle mission, i.e., with respect to range, mission time, and
 251 the thirty-second frequency.

252 When the topside tracking framework receives a message, with a time delay, Δt , it will
 253 request a new estimate for $c_{i,j}$ along with its standard deviation. The effective sound speed
 254 is predicted using the vehicle's reported depth and the extrapolated navigation solution for
 255 range, \hat{r} , as inputs to the ray tracing program, which returns an impulse response estimate
 256 in the form of ray travel times dt_j and amplitudes a_j .

257 The initial call to BELLHOP is over a local grid centered at the range and depth posited
 258 by the onboard tracking solution. The grid, compared to a point solver, adds redundancy
 259 in resolving the actual multipath structure for a reliable acoustic path without overtaxing
 260 onboard computational time and memory. It is initialized as 11×11 points spanning 10
 261 m horizontally and 20 m vertically. The horizontal dimension reflects the accumulated
 262 vehicle position error given a thirty-second communication cycle; the vertical dimension
 263 reflects how, computationally, eigenrays of the same timefront seem to stack vertically in
 264 the water column. For each grid point, BELLHOP produces a number of arrivals resulting
 265 from multiple propagation paths. Using only the N_0 rays with neither surface nor bottom
 266 bounces, it will then estimate the current effective sound speed c from a power weighted
 267 average of the ray travel times,

$$c = \frac{\hat{r} \sum_{n=1}^{N_0} a_n^2}{\sum_{n=1}^{N_0} dt_n a_n^2}, \quad (1)$$

268 and the associated weighted standard deviation,

$$\sigma_c \simeq \sqrt{\frac{\sum_{n=1}^{N_0} (dt_n - \hat{r}/u)^2 a_n^2}{\sum_{n=1}^{N_0} a_n^2}} \frac{u^2}{\hat{r}} \quad (2)$$

²⁶⁹ If no direct paths exist, i.e. $N_0 = 0$, then the effective speed is computed using the same
²⁷⁰ algorithm for the ray arrivals with one bounce, and so on.

²⁷¹ Finally, the pseudorange is calculated simply as

$$r_{i,j} = c_{i,j} \Delta t_{i,j} \quad (3)$$

²⁷² Thus the MBC method assumes the signal detected by the modem will be dominated by
²⁷³ a set of paths with the least number of boundary interactions. Importantly, this stochastic,
²⁷⁴ ensemble method for group velocity calculation can run in real-time, appearing to be orders
²⁷⁵ of magnitude faster than other post-processing methods which seek to determine the specific
²⁷⁶ ray itself that best matches a prominent indicator from the arrival structure. The BELLHOP
²⁷⁷ simulation that runs this calculation uses 3600 rays with launch angle fan of -60 to 60 degrees,
²⁷⁸ a representative depth dependent sound speed profile, and a range dependent bathymetry.

²⁷⁹ B. Pseudorange error metrics

²⁸⁰ The sister modem experiment generated 811 beacon to beacon communication events with
²⁸¹ their own real-time MBC group velocity predictions. Given the complexity of the ICNN
²⁸² system, this experiment did not collect an exhaustive set of data across all buoy, source
²⁸³ depth, receive depth, and sound speed combinations. The algorithm generally overestimates
²⁸⁴ pseudoranges because it resolves the effective sound speed for the most direct path.

²⁸⁵ Fig. 5 shows the range error boundary for both SSP inputs used in ICEX20. A promising
²⁸⁶ sign that the MBC method adapts sound speed somewhat intelligently is the lack of error
²⁸⁷ growth as travel time increases. The baseline SSP ($n=243$ events) has an absolute pseudor-

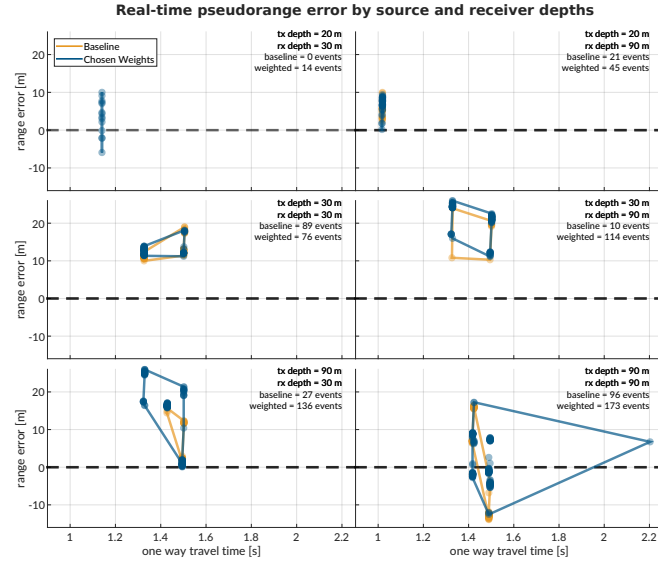


FIG. 5. The real-time range error by source (rows: 20, 30, and 90 m) and receiver (columns: 30 and 90 m) pairings for both sound speed estimates used during ICEX20. The amount of communication events is notated in the top right of each panel. The dashed line indicates no range error, and the boundary drawn indicates scope of the range error as a function of one way travel time.

ange error of 11.38 ± 4.23 m; the weighted SSP ($n=568$), 11.36 ± 8.12 m. The discrepancy between these two is largely due to outlier events only contained in the weighted SSP set. Where there is overlap between sound speed conditions used for the real-time MBC, the pseudorange error difference is no more than a few meters. The overarching results show that sound speed estimates derived from eigenrays for a local grid, as opposed to a singular point, are accurate enough to support vehicle navigation. While the NBC looks for just the least complex multipath, the high density of launch angles almost always guarantees a direct path. Nonetheless, the consistent overestimation of pseudorange invites further analysis into acoustic arrival matching.

297 **C. Eigenray identification for beacon-to-beacon events**

298 Accounting for ice movement between beacons creates nominal ranges with small vari-
 299 ability. Figs. 6, 7, and 8 show eigenrays for three sound speed environments for source
 300 depths of 20, 30, and 90 m, respectively. Eigenrays were initially found using the built-in
 301 BELLHOP protocol with a launch angle fan of 2400 rays between -60 and 60 degrees. Sepa-
 302 rately, recorded travel times between beacons were clustered with 1 millisecond boundaries
 303 such that some source-receiver pairs had multiple, distinct travel times to approximate. The
 304 BELLHOP eigenray returns were then filtered such that one was selected per travel time
 305 cluster, in the hopes that the eigenray will converge to the receiver locations for the most
 306 realistic sound speed input. It should be noted that bottom bounces were recovered but
 307 filtered out. The three source depths create distinct ray geometries with respect to the three
 308 sound speed inputs.

309 **1. Source depth of 20 m**

310 For a source at 20 m in depth, shown in Fig. 6, reliable eigenrays are found for all sound
 311 speed inputs. Rays refract upwards and neatly intersect with the shallow and deep receiver
 312 locations between 1.5 and 1.8 km in range. However, the ray paths for the shallow receivers
 313 change both in the number of surface interactions and where the surface interactions occur
 314 with respect to range across the SSPs. As the Beaufort Lens strengthens, the chosen paths to
 315 the second farthest shallow buoy (North, in red) interact with the surface more and become
 316 distinct. The weighted SSP shows the most interesting effects for the deeper receivers. The

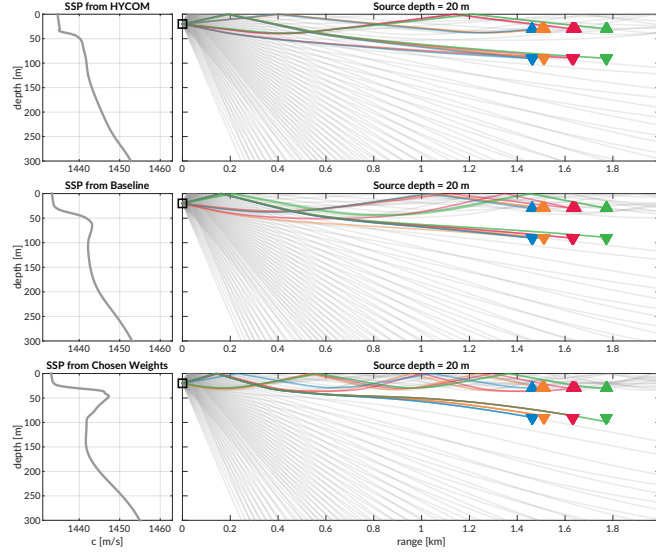


FIG. 6. Eigenrays for beacon-to-beacon events for each sound speed with a nominal source depth of 20 m over a total ray fan in gray. The beacons are highlighted in color/marker coding in Fig. 4.

317 ray paths all interact with the surface and the eigenrays for the Northern (red) and Western
318 (green) buoys are in fact the same ray.

319 2. Source depth of 30 m

320 The ray geometries from the 30 m source, shown in Fig. 6, show a similar degradation
321 of eigenray identification with increased ducting. Receptions span 1.5 to 3.2 km. Once
322 again, eigenrays for HYCOM and the baseline SSP are visually appropriate. Rays for the
323 weighted SSP show how the surface channel intensifies ice interactions and how the shadow
324 zone denies reliable acoustic paths. Pointedly, the increasing number of surface reflections to
325 the farthest shallow buoy (North, in red) crystallize the MBC's tendency for overestimation.
326 For the HYCOM, baseline, and weighted SSP inputs, the most appropriate eigenrays show
327 2, 3, and 4 surface interactions.

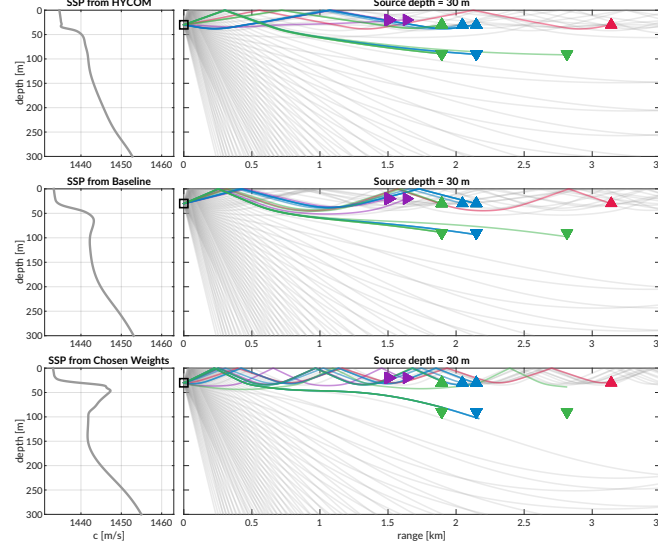


FIG. 7. Eigenrays for beacon-to-beacon events for each sound speed with a nominal source depth of 30 m over a total ray fan in gray. The beacons are highlighted in color/marker coding in Fig. 4.

328

3. Source depth of 90 m

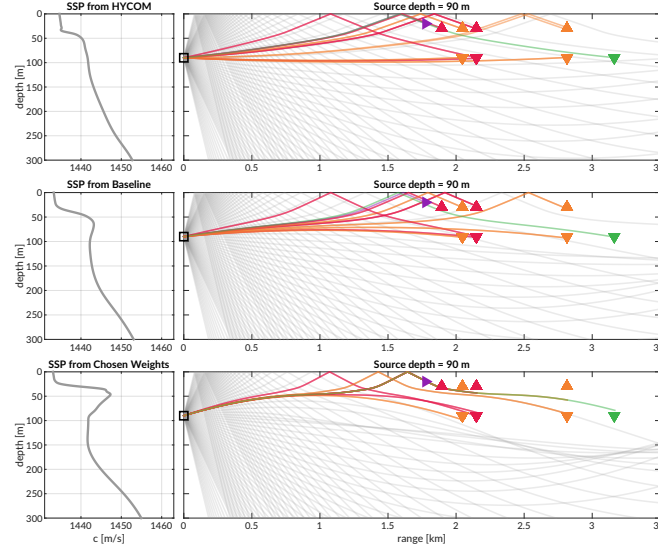


FIG. 8. Eigenrays for beacon-to-beacon events for each sound speed with a nominal source depth of 90 m over a total ray fan in gray. The beacons are highlighted in color/marker coding in Fig. 4.

329 Lastly, Fig. 8 shows ray geometries from the 90 m source, elucidating a different extent
330 of the shadow zone. While the receiver locations are similar to that of the 30 m source
331 depth, the deeper source depth effectively negates the upper duct and places the upper (and
332 some of the lower) receivers in unreliable acoustic paths. The HYCOM eigenrays still show
333 the most reliable acoustic paths that deteriorate with increasing ducted conditions. The
334 lack of direct paths from the observed SSP further points out the shortcomings of the MBC
335 approach.

336 The goal of the MBC algorithm was to provide a reliable, physically intuitive interpre-
337 tation of the acoustic propagation without taking on the additional burden of regularly
338 identifying specific paths that may connect any given source-receiver pair in the network.
339 While it was unlikely to resolve multipath arrivals that triggered successful modem detec-
340 tion, an isovelocity approach would have provided no adaptivity against source and receiver
341 depth differences. Its performance was adequate for vehicle navigation and would have likely
342 sufficed if it were not for the prominence of the duct observed relative that of other model
343 and data products.

³⁴⁴ **IV. POST-PROCESSED PSEUDORANGE ANALYSIS**

³⁴⁵ From all events recorded during the modem test experiment, there are 1242 successfully
³⁴⁶ decoded beacon-to-beacon events. Thus, a post-processing analysis that emulates the real-
³⁴⁷ time navigation engine was run to overcome the unequal distribution of communication
³⁴⁸ events with respect to depth, range, and sound speed status.

³⁴⁹ It is important to note that the value for the extrapolated range, \hat{r} , is only tracked when
³⁵⁰ the modem runs the vehicle behavior; thus we replace \hat{r} with the GPS-tracked range for
³⁵¹ all modem events. Because \hat{r} converges to the correct solution, a comparison of \hat{r} with the
³⁵² GPS-tracked range shows a normal, zero-centered distribution within the bounds of GPS
³⁵³ drift. The analysis therefore seeds realistic but “omniscient” knowledge of the extrapolated
³⁵⁴ range and emulates the post-processing pipeline to more thoroughly evaluate the acoustic
³⁵⁵ pseudorange estimate for all modem events. Sound speed inputs are the isovelocity sound
³⁵⁶ speed in addition to the modeled, baseline, and weighted SSPs from Fig. 3. The analysis
³⁵⁷ replicates the MBC but also introduces a new filtering algorithm, the nearest bounce criteria
³⁵⁸ (NBC), based on insights gleaned from the eigenray analysis. Accordingly, the results in
³⁵⁹ this section evaluate the utility of the algorithms and sound speed sources, divorced from
³⁶⁰ their role in the ICNN while maintaining real-time relevance.

³⁶¹ **A. Nearest bounce criteria (NBC)**

³⁶² The extent of ray bending and repeated reflections is extremely dependent on the degree
³⁶³ of the Beaufort Lens observed. Based on this insight, a new algorithm, the nearest bounce

³⁶⁴ criteria (NBC), is a slight modification from the MBC and includes multipath as a new
³⁶⁵ dimension of information to exploit. This metric, while run in post-processing, adds a
³⁶⁶ negligible amount of computation for real-time efficacy.

³⁶⁷ Given a running estimate for the effective sound speed $c_{i,j}$ between nodes i and j , the
³⁶⁸ navigation system has an extrapolated value for range, \hat{r} , and a recorded travel time, $\Delta t_{i,j}$.
³⁶⁹ Instead of using only the N_0 rays with neither surface nor bottom bounces to estimate
³⁷⁰ conversion speed, and subsequently moving to incremental number of bounces only when no
³⁷¹ valid direct path solutions exist, we solve for the power weighted average of the ray travel
³⁷² time for the N_k rays with k bounces,

$$t_k = \frac{\sum_{n=1}^{N_k} dt_n a_n^2}{\sum_{n=1}^{N_k} a_n^2}, \quad (4)$$

³⁷³ find the nearest matching power weighted average to recorded travel time,

$$t_{i,j,k} = \min_{k=0,1,2,\dots} |t_k - \Delta t_{i,j}| \quad (5)$$

³⁷⁴ predict an effective sound speed,

$$c_{i,j} = \frac{\hat{r}}{t_{i,j,k}} \quad (6)$$

³⁷⁵ and estimate the range as was done previously.

$$r_{i,j} = c_{i,j} \Delta t_{i,j} \quad (7)$$

³⁷⁶ Whereas the MBC outputs a scalar, this method first outputs a vector of effective sound
³⁷⁷ speeds based on the number of reflections. Then a single value is selected that best matches
³⁷⁸ the recorded travel time, as the detected arrival is not always the first arrival or the direct
³⁷⁹ path and could even be masked by noise or blocked temporarily ([Deffenbaugh *et al.*, 1996b](#)).

³⁸⁰ We manually cap the number of bounces at four because of the smaller operational scale and
³⁸¹ the attenuation accrued with many surface interactions. Bottom bounces are not encoded
³⁸² separately because of ray's tendency to refract upward, not due to information limitations.

³⁸³ **B. Effective sound speed predictions**

³⁸⁴ The minimal and nearest bounce algorithms are applied with the three sound speed inputs
³⁸⁵ shown in Figs. 6, 7, 8. The resulting predicted effective sound speeds are shown in Fig. 9
³⁸⁶ for all source depths versus one way travel time.

³⁸⁷ The goal of the effective sound speed prediction is to converge towards the implied sound
³⁸⁸ speed, i.e. the GNSS-derived range divided by the recorded travel time. As the environ-
³⁸⁹ mental and ray filtering method become better representations of the real ocean, the lower
³⁹⁰ the expected mismatch is between the implied and estimated effective sound speeds.

³⁹¹ The various sound speed inputs—isovelocity aside—not only modify the predicted effec-
³⁹² tive sound speed, as seen by the colored vertical offsets, but often classify a distinct number
³⁹³ of bounces. HYCOM sees the most direct and one bounce multipath structures, lending a
³⁹⁴ bias for faster speeds; the weighted SSP sees the most double and triple bounces, favoring
³⁹⁵ slower speeds; the baseline sound speed exists in between. Very rarely is the multipath
³⁹⁶ structure classified as a direct path, where the MBC and NBC would prediction overlap. In
³⁹⁷ fact, the higher the multipath classification, the more accurate the sound speed prediction
³⁹⁸ is, likely driven by a tighter or even sparser bundle of rays. Discontinuities in multipath
³⁹⁹ classification provide initial evidence for its importance to a smoothly varying group veloc-
⁴⁰⁰ ity, as shown in the cluster of 30 to 30 m transmissions, where HYCOM jumps from one to

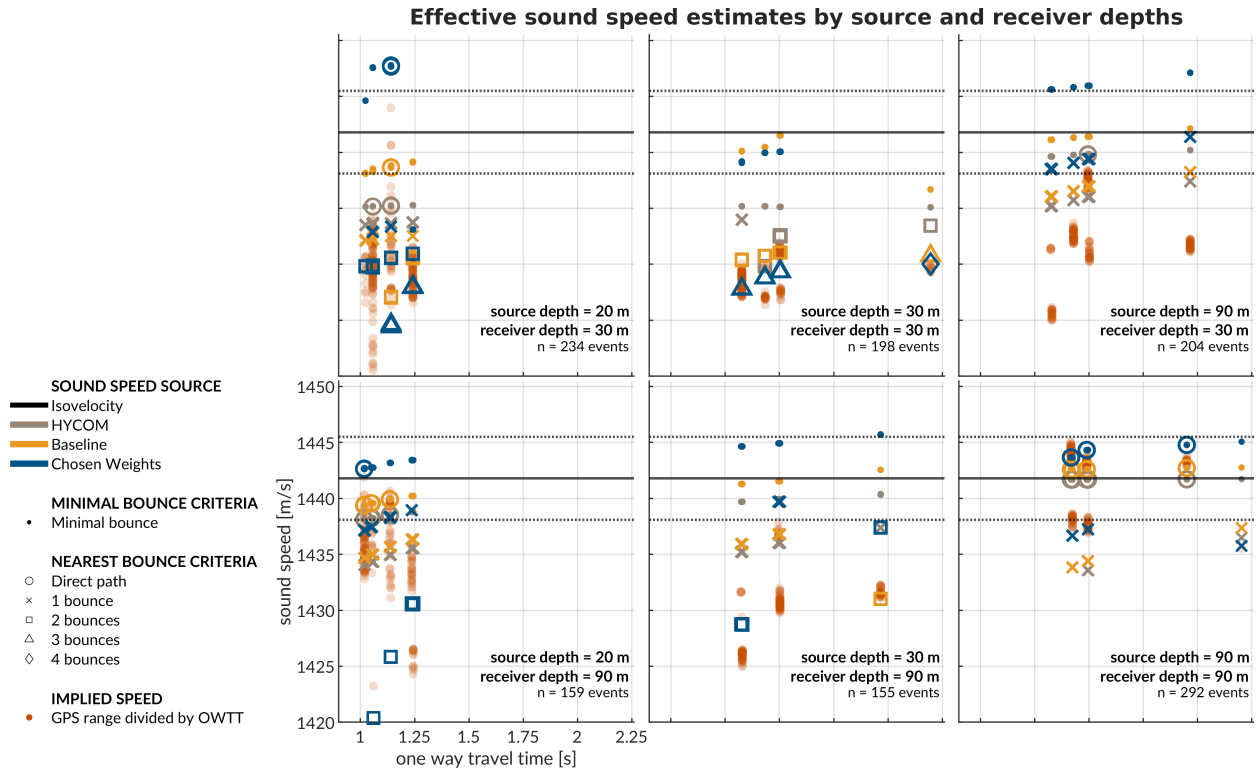


FIG. 9. A post-processing comparison of effective sound speed predictions for all beacon-to-beacon events. The rows share receiver depth; the columns share source depth. The recorded travel time is on the x-axis and the predicted effective sound speed is on the y-axis. The sound speed source is indicated by color. The isovelocity is shown as the mean \pm the standard deviation. The minimal and nearest bounce criterion are distinguished by different marker shapes, compared to the separately colored red dots showing the implied calculation.

401 two classified bounces amidst the baseline SSP and weighted SSP smoothly increasing while
 402 consistently seeing two and three classified bounces, respectively. Of course, the prediction
 403 deteriorates with cross-layer transmissions across the duct, but not to the same degree at
 404 which eigenrays could not be found for the weighted SSP in section III C. The evidence sug-

⁴⁰⁵ gests that the grid based method provides a useful amount of redundancy to resolve similar
⁴⁰⁶ enough eigenrays.

⁴⁰⁷ It is useful to think about in what case the isovelocit—or any isovelocit framing—would
⁴⁰⁸ have been appropriate. The transmissions from shallow to shallow receiver would may have
⁴⁰⁹ matched the default configuration of 1430 m/s. The isovelocit contrived for this paper,
⁴¹⁰ 1441.8 m/s, best matches the transmissions from 90 to 90 m. The one from [Graupe *et al.*](#)
⁴¹¹ ([2019](#)), 1450 m/s, would have had a systemic overestimation. Given that implied sound
⁴¹² speeds just for beacon-to-beacon events span 1420 to 1445 m/s, it is safe to say that a
⁴¹³ nominal sound speed would sacrifice pseudorange accuracy somewhere, and that an adaptive
⁴¹⁴ approach is necessary even for short range operations in the Beaufort Lens.

⁴¹⁵ **C. Pseudorange error metrics**

⁴¹⁶ Pseudorange estimation plays an important role in trilateration. Fig. [10](#) shows the
⁴¹⁷ directional pseudorange error “footprints” for the four sound speed inputs with the NBC
⁴¹⁸ approach, separated by source and receiver depth configurations.

⁴¹⁹ The weighted SSP range error generally has the smallest and most zero-centered footprint.
⁴²⁰ The one case it does not is for the source-receiver pairings between 30 and 90 m in depth. The
⁴²¹ increased error for these is most likely driven by the computational artifacts encountered
⁴²² when propagating through the steep sound speed gradients of the lens and through the
⁴²³ shadow zone. All other source depth pairings are significantly improved using the chosen
⁴²⁴ weights compared to HYCOM or the baseline.

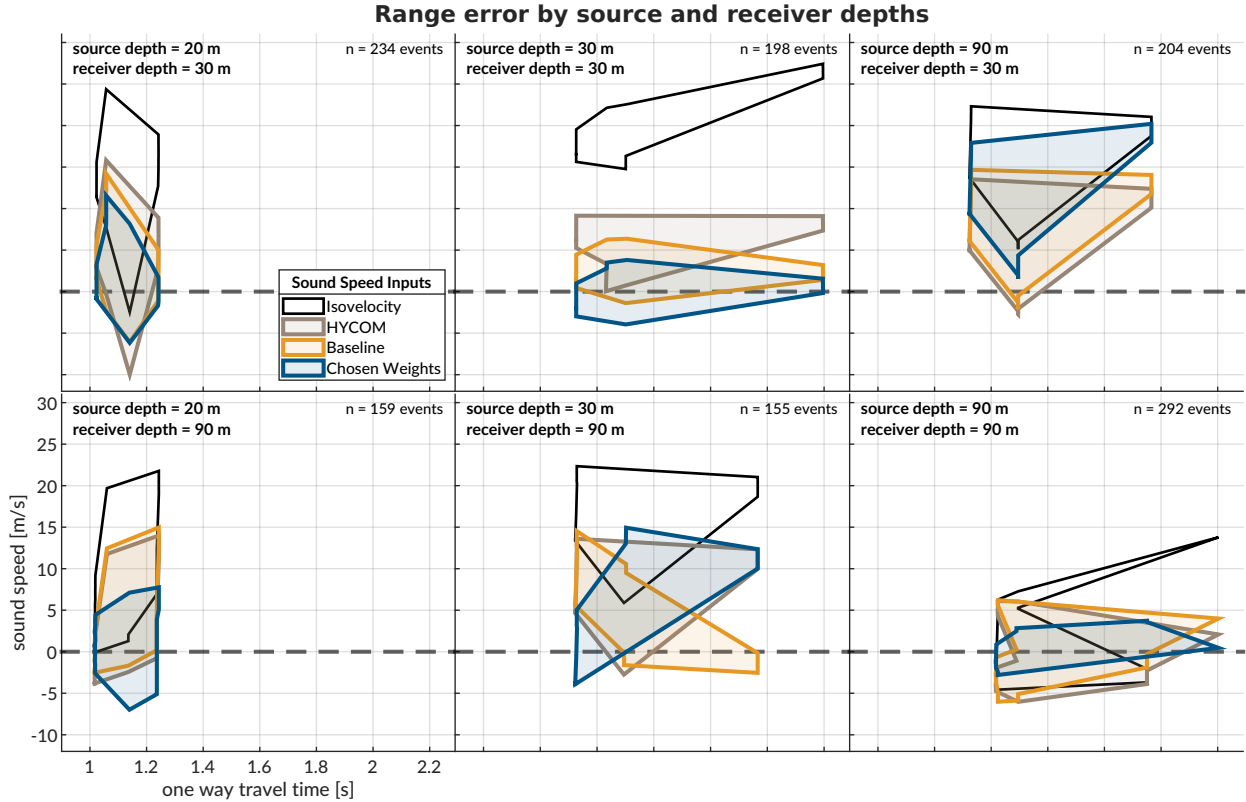


FIG. 10. The post-processed pseudorange error; the rows share receiver depth; the columns share source depth. The dashed gray line shows no error. The shaded region connects the range performance across all events.

When using a linear scaling to convert travel time into range, any offset between the assumed sound speed and the horizontal group velocity produces unconstrained error with increasing receiver distance, whereas an adaptive estimate would exhibit no such trend. This is easily observed in the same-layer links, i.e., 30 to 30 m and 90 to 90 m. In cross-layer links, the isovelocity does not perform better but tends to exaggerate or flip the footprint created adaptively.

The improvement from MBC to NBC is most evident for the data-driven sound speed; while the HYCOM SSP improves from a median absolute range error of 6.41 to 4.61 m,

433 the baseline SSP improves from 10.30 to 2.27 m, and the weighted SSP improves from
434 13.28 to 2.12 m. In comparison, the isovelocity has a median error of 13.09 m. The order
435 of magnitude improvement in the ducted SSPs demonstrate the effectiveness of the NBC
436 algorithm exploiting the observed multipath conditions.

437 There is one example that helpfully illustrates the improvement brought upon by bounce
438 classification. For transmissions between North and South at 30 m, the OWTT spread is
439 2.1958 to 2.1963 s; the GNSS-tracked distance is 3138.54 to 3140.87 m; and the implied
440 effective sound speed is 1429.3 to 1430.1 m/s. For these transmissions, the weighted SSP
441 and the MBC approach produce a pseudorange error of -1491 m, as the effective sound speed
442 is dominated by bottom bounce arrivals with much greater travel times. The NBC approach
443 categorizes this same record as a quadruple surface bounce, reducing the pseudorange error
444 to less than a meter. Comparatively, the NBC approach for HYCOM and the baseline
445 SSP produce pseudorange errors of 8.30 and 2.39 m, respectively. There is strong evidence
446 to suggest that the sound speed and multipath fidelity codependently improve localization
447 accuracy.

⁴⁴⁸ **V. TRILATERATION FOR ICEX20 FIELD DATA**

⁴⁴⁹ To overcome potentially intermittent acoustic communication, the operational paradigm
⁴⁵⁰ of the ICNN computes corrections relative to the trilaterated position estimates transmitted
⁴⁵¹ by the vehicle, rather than transmitting the updated positions themselves. The reliability of
⁴⁵² the correction is directly linked to how accurately the travel time measurements are converted
⁴⁵³ to pseudoranges. This section aims to resolve that tension by reevaluating the trilateration
⁴⁵⁴ results with respect to the MBC and NBC algorithms. The MBC/NBC effective speed
⁴⁵⁵ predictions were tracked independently for each source-receiver pair; although the sound
⁴⁵⁶ speed was expected to be locally smooth near a given receiver, no such assumption was
⁴⁵⁷ enforced between distinct acoustic links.

⁴⁵⁸ **A. Re-positioning beacon to beacon events**

⁴⁵⁹ When the beacons ran as virtual vehicles, the ICNN did not have access to that buoy's
⁴⁶⁰ GPS data stream except for what was sent via digital acoustic message. The static nature of
⁴⁶¹ the experiment means that the initial estimate transmitted to the ICNN was in fact a ground
⁴⁶² truth position. Therefore, a distribution of corrections from the ICNN, as shown in Fig. 11,
⁴⁶³ reflects positioning accuracy. The NBC clearly outperforms the MBC, with almost 80% of
⁴⁶⁴ the corrections below 6 meters and the median within the deployed GNSS puck precision
⁴⁶⁵ of 3 meters. By contrast, the MBC shows roughly 20% within the GNSS puck precision,
⁴⁶⁶ and separate peaks from 9–12 meters and 21–27 meters. This trimodal nature reflects the
⁴⁶⁷ distribution of reflections on the ice surface.

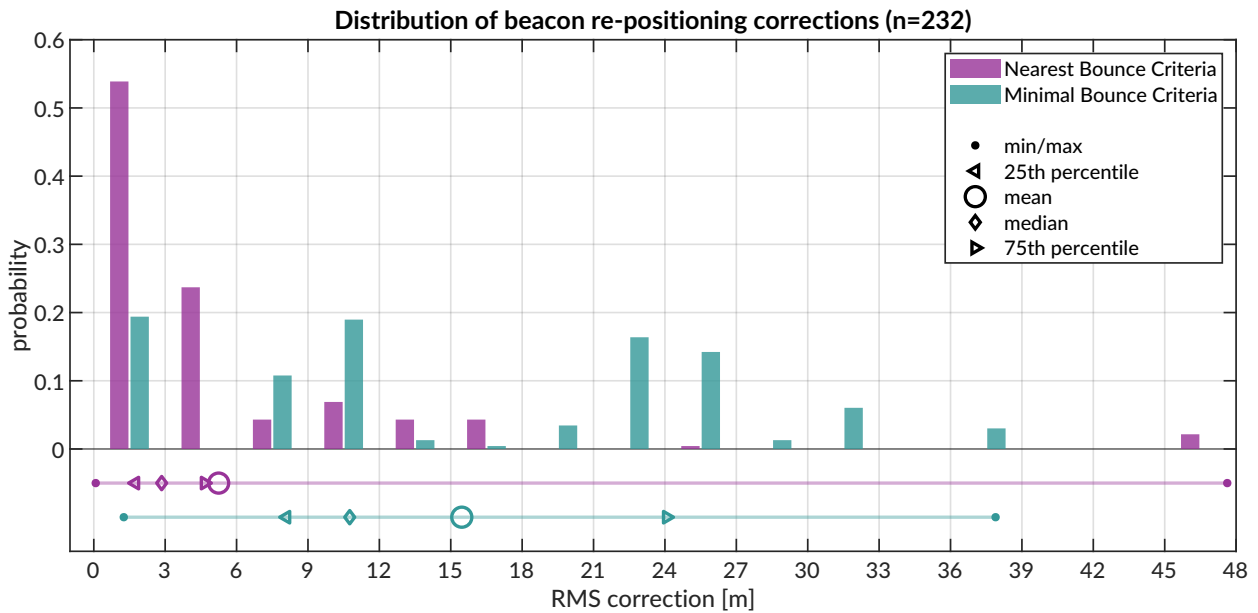


FIG. 11. Trilateration events; however, 264 entries are 2-beacon solutions, 22 are 3-beacon, and 2 are 4-beacon. When limited to only two ranging circles, the trilateration chooses the closer of the two intersection points. The x-axis is cut off at the upper limit for the NBC algorithm.

468 In several events, the MBC is unable to accurately estimate the effective sound speed for
 469 one of the acoustic links, leading to a large positioning error. The NBC, however, better
 470 resolves an approximation of the acoustic path. For example, in some trilateration solutions
 471 for the Eastern buoy, the MBC shows a correction of more than a kilometer; the NBC is
 472 two orders of magnitudes less.

473 **B. Re-navigating AUV *Macrura***

474 Up to this point, pseudorange estimation and localization have been evaluated on GPS-
 475 linked beacon-to-beacon connections to validate the NBC algorithm. This analysis ports the
 476 MBC and NBC algorithms to re-navigate the AUV *Macrura*.

477 In comparison to the modem experiment, the AUV data clearly exhibit instances where
 478 a receiver detects the same transmission more than once. This is not surprising considering
 479 the complex multipath provided by the Beaufort Lens. The 11 hour vehicle mission con-
 480 tains 3,260 transmissions, 12,938 total detections, and 4,704 successful receptions. Allowing
 481 receptions with PSK errors would almost double the number of recorded multipath arrivals
 482 exploited for positioning, if a real-time solution could correctly parse paths from different
 483 arrivals in the same thirty-second cycle. Thus it remains a future endeavor to explore how
 484 failure mode information from acoustic modems could be used to identify unsuccessful but
 485 otherwise trustworthy arrivals to augment trilateration samples.

486 The following performance analysis is constrained to what the vehicle acted on in real-
 487 time. AUV *Macrura* and the ICNN ran an adaptive depth behavior to maintain acoustic
 488 communication on the insight that cross-layer links were more likely to fail than same-layer
 489 ones. Accordingly, the vehicle dove deeper than 50 meters about 20% of the time it was
 490 underway.

491 In contrast to the modem tests, where position correction illustrated re-positioning ac-
 492 curacy, the re-navigation corrections are less valuable in the absence of GNSS ground truth.
 493 The correction magnitude necessarily depends on the vehicle's internal navigation estimate,
 494 which is prone to larger errors from sensor drifts, ocean currents, and other error not cap-
 495 tured in the hydrodynamic model. Thus, larger corrections are not necessarily indicative of
 496 worse performance. Navigation accuracy is better described by trilateration error, the RMS
 497 of the remaining pseudorange errors from each acoustic link.

498 Fig. 12 shows the correction magnitudes and trilateration errors for events with three or
 499 more receptions during AUV operations. Whereas the MBC has a fairly bimodal nature,
 500 with peaks centered around 10–15 and 35–40 m, the NBC favors smaller corrections, from
 501 5–20 m, and has a long tail. The distribution of corrections are much larger than the
 502 distribution of RMS error. It is apparent that, while both methods are quite successful,
 503 there is strong evidence that the NBC achieves single meter accuracy.

504 **C. Investigating potential GNSS noise**

505 The fact that the bulk of the best performing re-navigation error exists within the pre-
 506 cision of the GNSS unit deployed invites a further look into GNSS noise. In the Arctic,
 507 GNSS performance worsens due to poor constellation coverage, larger ionospheric effects,
 508 and multipath interference. The National Security Implications of Climate Change for U.S.
 509 Naval Forces (Council, 2011) details some of the limitations of the Global Positioning Sys-
 510 tem (GPS) at polar latitudes. Radio infrastructure that provides position corrections and
 511 references does not regularly extend to polar regions. The effect is minor for surface plat-
 512 form navigation —roughly 15 m of horizontal precision has been displayed at the North
 513 Pole—but is significant enough to register against the modem’s detected travel times. Fig.
 514 13 zooms in on the GNSS and OWTT noise relative to the ice movement for two pairs of
 515 modem buoy connections. The two panels indicate the GPS drift as $\delta R = \sqrt{\delta x^2 + \delta y^2}$ and
 516 temporal drift, δt , relative to the median OWTT recorded between the two modems. The
 517 dashed line is scaled by a group velocity of 1440 m/s, such that if there were ideal sensor
 518 measurements with no drift, all events should exist on or near the line.

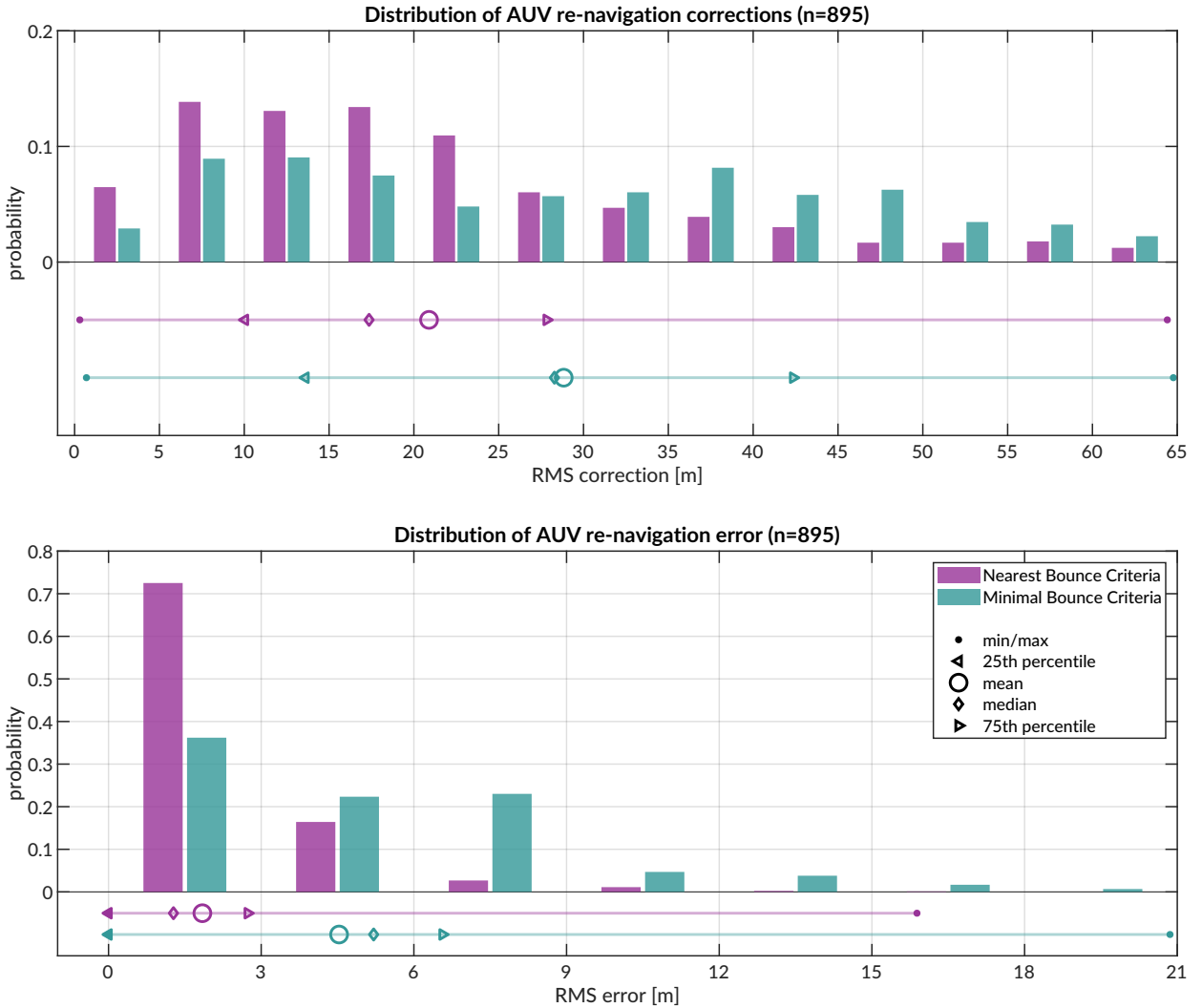


FIG. 12. Distribution of vehicle re-navigation corrections (top) and error (bottom) computed in post-processing for the Minimum and Nearest Bounce Criterion.

519 The top panel shows the connections between the North and East buoys. The clusters
 520 scaling along the 1440 m/s guideline suggest relative ice movement picked up by both GNSS
 521 and OWTT. But the vertical distribution across many arrival time bands is indicative of
 522 the GNSS fluctuations in precision, or noise. Some minor offsets between these vertical
 523 bands relate to different operational configurations of source and receiver depth. The idea

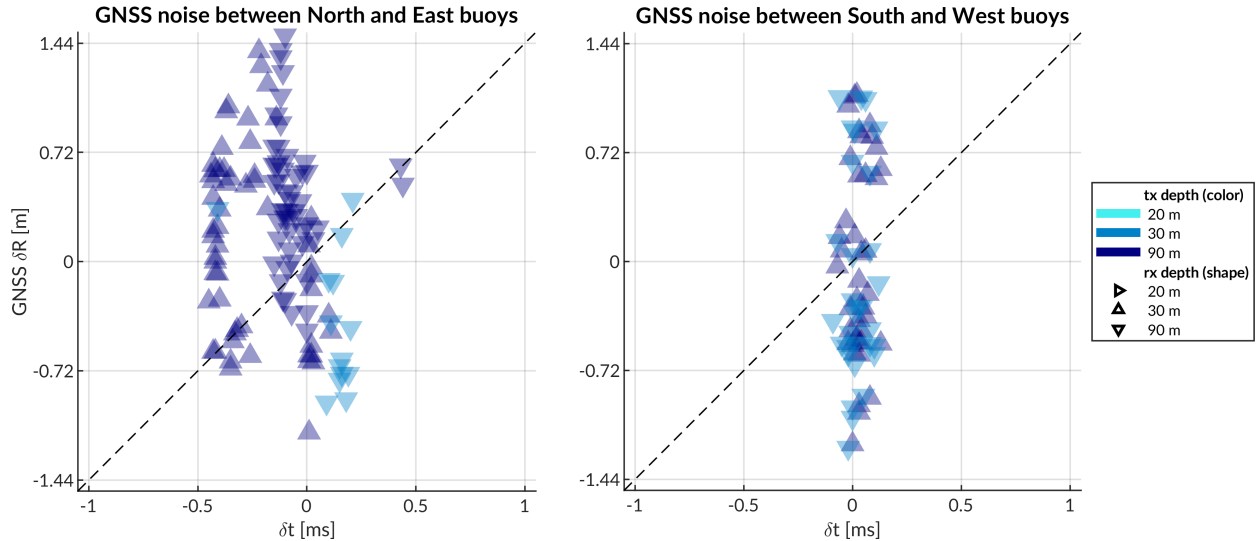


FIG. 13. A comparison of GPS drift (y-axis) versus OWTT drift (x-axis) for corners of the ICNN network with different source depths.

524 of GNSS noise relative to OWTT is further indicated by events between two other buoys,
 525 South and West. The relatively thin time window suggests these buoys are moving in
 526 a more rigid ice floe and that there is minimal impact by source and receiver depth on
 527 the spread of OWTT. Yet, the vertical distribution, spanning almost 4 meters, cannot be
 528 explained by time differentials due to acoustic scattering, multipath, and/or environmental
 529 microstructure. This conclusion corroborates the vertical spread of implied effective speeds
 530 in Fig. 9.

531 **VI. DISCUSSION**

532 Underwater navigation research is broadly motivated by acquiring GNSS-like navi-
 533 gation in GNSS-denied conditions. Accurate range estimation is essential to mitigating error.
 534 Current approaches for underwater acoustic navigation simplify the non-linear relationship
 535 between a SSP and timefronts with a deterministic sound speed. Thus, the conversion of
 536 travel time into distance can be pre-conditioned for error and error growth over the course
 537 of a vehicle mission. This work introduces a lightweight stochastic prediction of an effec-
 538 tive sound speed along the path between source and receiver, retooling arrival methods
 539 generally deemed too complex or labor intensive for real-time. We assume that the effec-
 540 tive sound speed would be a locally smoothly varying function with respect to operational
 541 conditions—horizontal and vertical differences and rate of difference between source and re-
 542 ceiver. The field-tested approach, the minimal bounce criteria, facilitated a successful AUV
 543 recovery in a total ice-covered, double ducted environment. The accuracy of the MBC was
 544 validated against GPS-linked beacon-to-beacon communications. Given a consistent bias
 545 towards overestimation, an improved algorithm, the nearest bounce criteria, was developed
 546 on the insight that multipath structure may play an outsized role in maintaining a smoothly
 547 varying effective sound speed. The NBC was developed with field data and reevaluated on
 548 vehicle data, achieving a position accuracy and precision that rivals that of the deployed
 549 GNSS puck.

550 A key insight for both approaches was seeking an eigenray ensemble around an estimated
 551 location instead of seeking to unambiguously match arrivals. The ensemble diversified the

552 simulated multipath possibilities to better capture the actual multipath recorded. In this
553 way, the solution exploits multipath, generally viewed as a source of uncertainty, as a new
554 dimension of information to improve localization accuracy. Based on the navigation and re-
555 navigation results of our AUV deployment in the ice-covered Beaufort Sea, we conclude that
556 embedding a model-aided prediction of the effective sound speed has an outsized benefit
557 to minimizing trilateration error, and that our approach sufficiently resolves the acoustic
558 timefronts for an unpredictable, complex propagation environment like the double ducted
559 Beaufort Lens.

560 There are many avenues through which this approach can be further refined and tested for
561 field operations. Amongst them is defining the uncertainty grid for BELLHOP via stochastic
562 or data-driven measures such as the distance traveled by the AUV between ICNN updates
563 or the magnitude of the position corrections by the ICNN. Another is to entirely remove the
564 seeded range and instead rely on the submerged asset's depth and recorded OWTT to find
565 high probability fields in range.

566 The relatively simple nature of this approach suggests it is transferable to other envi-
567 ronments, spatio-temporal scales, and platforms. While it is likely a particular quirk of
568 the Beaufort Lens that filtering for reflection alone can produce a horizontal effective speed
569 that compensates for ray refraction and reflection, it is trivial to filter along other ways, like
570 number of turning points, to create a more diverse and informed set of multipath timefronts.
571 Though the majority of re-navigation results are within single-meter accuracy, future work
572 can examine how constellations of more LBL beacons can extend the operational domain
573 without adding an undesirable amount of error. One possibility is that, during a mission,

574 ICNN-like LBL implementations use a comparison of the GNSS self-position and acoustic po-
 575 sitioning to invert for the ocean volume, linking how vertical and horizontal sound speed
 576 structure impact transmission integrity. A fast tomographic estimate ([Deffenbaugh, 1997](#);
 577 [Elisseeff *et al.*, 2002](#)), along with its uncertainty, can be continuously communicated to assets
 578 underway to maintain contact or enable adaptive sampling. In this sense navigation and to-
 579 mography converge on the same set of component technologies—position estimation, sound
 580 speed parameterization estimation, ray path identification, and vehicle path optimization.

581 Spatio-temporal variability is a serious challenge for accurate real-time ranging. On
 582 one hand, the effectiveness of eigenray filtering algorithm is likely only challenged by the
 583 valid operational scales of a range independent propagation environment. Longer range
 584 experiments may provide more time for eigenray filtering. A bootstrapping approach that
 585 filters eigenrays for several randomly generated internal wave spectrums may compensate
 586 for otherwise unknowable spatio-temporal variability. The model-aided component to the
 587 eigenray filtering is compatible with vertical slices from any physically driven ocean model.
 588 But in the long run, more accurate and higher resolution global circulation models are
 589 needed to properly resolve features that alter ducted propagation at the scales discernible
 590 to an acoustic modem. Through-the-sensor methods can resolve local features but would
 591 require a degree of information sharing not readily supported on the acoustic channel for
 592 large scale variability. But addressing the spatial and temporal scales of what can be solved
 593 deterministically and what must be solved stochastically imposes a resolution constraint
 594 that is at odds with computational overhead for real-time operations. Resolving features
 595 inaccurately, or with a false sense of confidence, could be more harmful than contextualizing

596 the limitations of a range independent propagation over realistic bathymetry. Given that
597 AUV operations are often on smaller spatial and temporal scales, the added benefit of a
598 gridded model is quite small, and for features like the Beaufort Lens, not well resolved.

599 The methods presented in this paper, including the software projects ([Benjamin *et al.*, 2010](#);
600 [Schneider *et al.*, 2015](#); [Schneider and Schmidt, 2010](#)), are open source and platform
601 agnostic. Large AUVs, often large enough to support long duration and/or deep sea mis-
602 sions, would benefit from including diurnal or tidal effects for ranging. Gliders, though
603 generally low power and memory, have been equipped with acoustic modems. Their in-
604 ability to maintain position within a region of reliable acoustic path makes the impact of
605 an environmentally adaptive pseudorange estimation disproportionately positive. The ex-
606 act adjustments to the ensemble eigenray filtering are predicated on the expected sound
607 speed conditions and acoustic arrival structure; the problem is ripe application for other
608 simulation testbeds or machine learning methods. The continued development of embed-
609 ded acoustic processing on heterogenous platforms is fundamental to support a universal
610 underwater navigation scheme comparable to GNSS.

611 **ACKNOWLEDGMENTS**

612 We acknowledge the significant operational effort spearheaded by the LAMSS ICEX20
 613 team and all our collaborators. Bhatt was funded by a National Defense, Science, and
 614 Engineering Graduate Fellowship. This work was supported by the Office of Naval Research
 615 322-OA under ICEX20 (N00014-17-1-2474) and Task Force Ocean (N00014-19-1-2716).

616

617 Ballard, M. S., Badiey, M., Sagers, J. D., Colosi, J. A., Turgut, A., Pecknold, S., Lin, Y.-T.,
 618 Proshutinsky, A., Krishfield, R., Worcester, P. F., and Dzieciuch, M. A. (**2020**). “Tem-
 619 poral and spatial dependence of a yearlong record of sound propagation from the Canada
 620 Basin to the Chukchi Shelf,” The Journal of the Acoustical Society of America **148**(3),
 621 1663–1680, <http://asa.scitation.org/doi/10.1121/10.0001970http://files/814/>
 622 [Ballardetal.-2020-Temporalandspatialdependenceofayearlongreco.pdf](#), doi: [10.1121/10.0001970](https://doi.org/10.1121/10.0001970).

623
 624 Barker, L. D. L., Jakuba, M. V., Bowen, A. D., German, C. R., Maksym, T., Mayer,
 625 L., Boetius, A., Dutrieux, P., and Whitcomb, L. L. (**2020**). “Scientific challenges and
 626 present capabilities in underwater robotic vehicle design and navigation for oceanographic
 627 exploration under-ice,” Remote Sensing **12**(16), 1–31, doi: [10.3390/RS12162588](https://doi.org/10.3390/RS12162588).

628 Bellingham, J., Leonard, J., Vaganay, J., Goudey, C., Atwood, D., Consi, T., Bales, J.,
 629 Schmidt, H., and Chryssostomidis, C. (**1995**). “Auv operations in the arctic,” in *Sea Ice
 630 Mechanics and Arctic Modeling Workshop*.

- 631 Benjamin, M. R., Schmidt, H., Newman, P. M., and Leonard, J. J. (2010). “Nested au-
 632 tonomy for unmanned marine vehicles with moos-ivp,” Journal of Field Robotics **27**(6),
 633 834–875.
- 634 Bhatt, E. C. (2021). “A Virtual Ocean framework for environmentally adaptive, em-
 635 bedded acoustic navigation on autonomous underwater vehicles,” Ph.D. thesis, Mas-
 636 sachusetts Institute of Technology and Woods Hole Oceanographic Institution Joint Pro-
 637 gram, <https://hdl.handle.net/1912/27309>, doi: [10.1575/1912/27309](https://doi.org/10.1575/1912/27309).
- 638 Bhatt, E. C., Howard, B., and Schmidt, H. (2022). “An Embedded Tactical Decision Aid
 639 Framework for Environmentally Adaptive Autonomous Underwater Vehicle Communica-
 640 tion and Navigation,” IEEE Journal of Oceanic Engineering .
- 641 Brooke, J. (1981). “Arcs (autonomous remotely controlled submersible),” in *Proceedings of*
 642 *the 1981 2nd International Symposium on Unmanned Untethered Submersible Technology*,
 643 IEEE, Vol. 2, pp. 28–28.
- 644 Chassignet, E. P., Hurlburt, H. E., Smedstad, O. M., Halliwell, G. R., Hogan, P. J., Wall-
 645 craft, A. J., Baraille, R., and Bleck, R. (2007). “The HYCOM (HYbrid Coordinate
 646 Ocean Model) data assimilative system,” Journal of Marine Systems **65**(1-4), 60–83, doi:
 647 [10.1016/J.JMARSYS.2005.09.016](https://doi.org/10.1016/J.JMARSYS.2005.09.016).
- 648 Chen, R., Poulsen, A., and Schmidt, H. (2019). “Spectral, spatial, and tem-
 649 poral characteristics of underwater ambient noise in the Beaufort Sea in 1994
 650 and 2016,” The Journal of the Acoustical Society of America **145**(2), 605–
 651 614, <https://asa.scitation.org/doi/full/10.1121/1.5088601http://files/757/>
 652 [Chenetal.-2019-Spectral, spatial, and temporal characteristics of.pdf](https:// Chenetal.-2019-Spectral, spatial, and temporal characteristics of.pdf), doi: 10.

- 653 1121/1.5088601.
- 654 Chen, R., and Schmidt, H. (2020). “Temporal and spatial charac-
 655 teristics of the Beaufort Sea ambient noise environment,” The Jour-
 656 nal of the Acoustical Society of America **148**(6), 3928–3941, <https://asa.scitation.org/doi/full/10.1121/10.0002955>
- 657 <https://files/755/ChenandSchmidt-2020-TemporalandspatialcharacteristicsoftheBeaufo.pdf>, doi:
 658 [10.1121/10.0002955](https://doi.org/10.1121/10.0002955).
- 660 Claus, B., Kepper, J. H., Suman, S., and Kinsey, J. C. (2018). “Closed-loop one-way-travel-
 661 time navigation using low-grade odometry for autonomous underwater vehicles,” Journal
 662 of Field Robotics **35**(4), 421–434, doi: [10.1002/rob.21746](https://doi.org/10.1002/rob.21746).
- 663 Council, N. R. (2011). *National Security Implications of Climate Change for U.S. Naval Forces* (The National Academies Press, Washington, DC), <https://www.nap.edu/catalog/12914/national-security-implications-of-climate-change-for-us-naval-forces>.
- 667 Deffenbaugh, M. (1997). “Optimal Ocean Acoustic Tomography and Navigation with Mov-
 668 ing Sources,” Ph.D. thesis, MIT-WHOI Joint Program in Oceanography/Applied Ocean
 669 Science and Engineering.
- 670 Deffenbaugh, M., Bellingham, J. G., and Schmidt, H. (1996a). “Relationship between
 671 spherical and hyperbolic positioning,” Oceans Conference Record (IEEE) **2**, 590–595, doi:
 672 [10.1109/OCEANS.1996.568293](https://doi.org/10.1109/OCEANS.1996.568293).
- 673 Deffenbaugh, M., Schmidt, H., and Bellingham, J. G. (1996b). “Acoustic positioning in a
 674 fading multipath environment,” in *OCEANS 96 MTS/IEEE Conference Proceedings. The*

- 675 *Coastal Ocean-Prospects for the 21st Century*, IEEE, Vol. 2, pp. 596–600.
- 676 Duda, T. F., Morozov, A. K., Howe, B. M., Brown, M. G., Speer, K., Lazarevich,
 677 P., Worcester, P. F., and Cornuelle, B. D. (2006). “Evaluation of a long-range joint
 678 acoustic navigation / thermometry system,” in *Oceans 2006*, pp. 1–6, <http://files/939/Dudaetal.-2006-EvaluationofaLong-RangeJointAcousticNavigati.pdf>
 679 <http://files/940/4099137.html>, doi: [10.1109/OCEANS.2006.306999](https://doi.org/10.1109/OCEANS.2006.306999).
- 680
- 681 Duda, T. F., Zhang, W. G., and Lin, Y.-T. (2021). “Effects of Pacific Summer Water layer
 682 variations and ice cover on Beaufort Sea underwater sound ducting,” The Journal of the
 683 Acoustical Society of America **149**(4), 2117–2136, doi: [10.1121/10.0003929](https://doi.org/10.1121/10.0003929).
- 684 Duda, T. F., Zhang, W. G., Lin, Y.-T., and Newhall, A. E. (2019). “Long-
 685 range sound propagation in the Canada Basin,” <http://files/565/Dudaetal.-Unknown-LONG-RANGESOUNDPROPAGATIONINTHECANADABASIN.pdf>.
- 686
- 687 Elisseeff, P., Schmidt, H., and Xu, W. (2002). “Ocean acoustic tomography as a data assimilation problem,” IEEE Journal of Oceanic Engineering **27**(2), 275–282, <http://files/438/Elisseeff,Schmidt,Xu-2002-OceanAcousticTomographyasaDataAssimilationProblem.pdf>, doi:
 688 [10.1109/JOE.2002.1002482](https://doi.org/10.1109/JOE.2002.1002482).
- 689
- 690
- 691
- 692 Eustice, R. M., Whitcomb, L. L., Singh, H., and Grand, M. (2006). “Recent advances in
 693 synchronous-clock one-way-travel-time acoustic navigation,” Oceans 2006 doi: [10.1109/OCEANS.2006.306931](https://doi.org/10.1109/OCEANS.2006.306931).
- 694
- 695 Eustice, R. M., Whitcomb, L. L., Singh, H., and Grund, M. (2007). “Ex-
 696 perimental results in synchronous-clock one-way-travel-time acoustic naviga-

- 697 tion for autonomous underwater vehicles,” in *Proceedings - IEEE International*
 698 *Conference on Robotics and Automation*, pp. 4257–4264, <http://files/877/Eusticeetal.-2007-ExperimentalResultsinSynchronous-ClockOne-Way-.pdf> <http://files/878/4209752.html>, doi: [10.1109/ROBOT.2007.364134](https://doi.org/10.1109/ROBOT.2007.364134).
- 700 Fossum, T. O., Norgren, P., Fer, I., Nilsen, F., Koenig, Z. C., and Ludvigsen, M. (2021).
 701 “Adaptive sampling of surface fronts in the arctic using an autonomous underwater ve-
 702 hicle,” *IEEE Journal of Oceanic Engineering* **46**(4), 1155–1164, doi: [10.1109/JOE.2021.3070912](https://doi.org/10.1109/JOE.2021.3070912).
- 703 Freitag, L., Ball, K., Partan, J., Koski, P., and Singh, S. (2016). “Long range acoustic
 704 communications and navigation in the Arctic,” *OCEANS 2015 - MTS/IEEE Washington*
 705 2–6, doi: [10.23919/oceans.2015.7401956](https://doi.org/10.23919/oceans.2015.7401956).
- 706 Graupe, C. E., Van Uffelen, L. J., Webster, S. E., Worcester, P. F., and Dzieci-
 707 uch, M. A. (2019). “Preliminary results for glider localization in the Beau-
 708 fort Duct using broadband acoustic sources at long range,” in *OCEANS 2019*
 709 *MTS/IEEE Seattle, OCEANS 2019*, pp. 1–6, <http://files/763/Graupeetal.-2019-Preliminaryresultsforgliderlocalizationinthe.pdf> <http://files/912/Graupeetal.-2019-Preliminaryresultsforgliderlocalizationinthe.pdf> <http://files/764/8962637.html> <http://files/913/8962637.html>, doi: [10.23919/OCEANS40490.2019.8962637](https://doi.org/10.23919/OCEANS40490.2019.8962637).
- 710 Hayes, D. R., and Morison, J. H. (2002). “Determining turbulent vertical velocity, and
 711 fluxes of heat and salt with an autonomous underwater vehicle,” *Journal of Atmospheric*
 712 *and Oceanic Technology* **19**(5), 759–779.

- 719 Howe, B. M., Miksis-Olds, J., Rehm, E., Sagen, H., Worcester, P. F., and Haral-
 720 abus, G. (2019). “Observing the Oceans Acoustically,” *Frontiers in Marine Science* **6**,
 721 426, <https://www.frontiersin.org/article/10.3389/fmars.2019.00426/full>, doi:
 722 [10.3389/fmars.2019.00426](https://doi.org/10.3389/fmars.2019.00426).
- 723 Jackson, E. (1983). “Autonomous remotely controlled submersible “ARCS”,” in *Proceedings*
 724 of the 1983 3rd International Symposium on Unmanned Untethered Submersible Technol-
 725 ogy, IEEE, Vol. 3, pp. 77–88.
- 726 Jakuba, M. V., Roman, C. N., Singh, H., Murphy, C., Kunz, C., Willis, C., Sato,
 727 T., and Sohn, R. A. (2008). “Long-baseline acoustic navigation for under-ice
 728 autonomous underwater vehicle operations,” *Journal of Field Robotics* **25**(11-12),
 729 861–879, <https://onlinelibrary.wiley.com/doi/full/10.1002/rob.20250>
 730 <https://onlinelibrary.wiley.com/doi/abs/10.1002/rob.20250>
 731 <https://onlinelibrary.wiley.com/doi/10.1002/rob.20250>, doi: [10.1002/ROB.20250](https://doi.org/10.1002/ROB.20250).
- 732 Kepper, J. H., Claus, B. C., and Kinsey, J. C. (2017). “MEMS IMU and one-
 733 way-travel-time navigation for autonomous underwater vehicles,” in *OCEANS*
 734 2017 - Aberdeen, Vol. 2017-Octob, pp. 1–9, <http://files/550/Kepper,Claus,Kinsey-2017-MEMSIMUandOne-Way-Travel-TimeNavigationforAutonomousUnderwaterVehicles.pdf>,
 735 doi: [10.1109/OCEANSE.2017.8084842](https://doi.org/10.1109/OCEANSE.2017.8084842).
- 737 Krishfield, R., Toole, J., Proshutinsky, A., and Timmermans, M. L. (2008). “Automated
 738 ice-tethered profilers for seawater observations under pack ice in all seasons,” *Journal of*
 739 *Atmospheric and Oceanic Technology* **25**(11), 2091–2105, doi: [10.1175/2008JTECH0587.1](https://doi.org/10.1175/2008JTECH0587.1).
- 740 1.

- 741 Kukulya, A., Plueddemann, A., Austin, T., Stokey, R., Purcell, M., Allen, B., Littlefield, R.,
- 742 Freitag, L., Koski, P., Gallimore, E. *et al.* (2010). “Under-ice operations with a remus-100
- 743 auv in the arctic,” in *2010 IEEE/OES Autonomous Underwater Vehicles*, IEEE, pp. 1–8.
- 744 Kunz, C., Murphy, C., Camilli, R., Singh, H., Bailey, J., Eustice, R., Jakuba, M., Nakamura,
- 745 K., Roman, C., Sato, T., Sohn, R., and Willis, C. (2008). “Deep sea underwater robotic
- 746 exploration in the ice-covered Arctic ocean with AUVs,” in *2008 IEEE/RSJ International*
- 747 *Conference on Intelligent Robots and Systems*, IEEE, pp. 3654–3660, <http://files/875/Kunzetal.-2008-Deepseaunderwaterroboticexplorationintheice.pdf>
- 748 <http://files/968/Kunzetal.-2008-Deepseaunderwaterroboticexplorationintheice.pdf>
- 749 <http://ieeexplore.ieee.org/document/4651097/>, doi: [10.1109/IROS.2008.4651097](https://doi.org/10.1109/IROS.2008.4651097).
- 750 Light, R., and Morison, J. (1989). “The autonomous conductivity-temperture vehicle: First
- 751 in the seashuttle family of autonomous underwater vehicle’s for scientific payloads,” in
- 752 *Proceedings OCEANS*, Vol. 3, pp. 793–798, doi: [10.1109/OCEANS.1989.586683](https://doi.org/10.1109/OCEANS.1989.586683).
- 753 Litvak, A. (2015). “Acoustics of the deepwater part of the arctic ocean and of russia’s
- 754 arctic shelf,” *Herald of the Russian Academy of Sciences* **85**, 239–250, doi: [10.1134/S1019331615030144](https://doi.org/10.1134/S1019331615030144).
- 755 Mikhalevsky, P. N., Sperry, B. J., Woolfe, K. F., Dzieciuch, M. A., and Worces-
- 756 ter, P. F. (2020). “Deep ocean long range underwater navigation,” *The Jour-*
- 757 *nal of the Acoustical Society of America* **147**(4), 2365–2382, <http://asa.scitation.org/doi/10.1121/10.0001081>
- 758 <http://files/631/Mikhalevsketal.-2020-Deepoceanlongrangeunderaternavigation.pdf>, doi: [10.1121/10.0001081](https://doi.org/10.1121/10.0001081).

- 763 Norgren, P., Lubbad, R., and Skjetne, R. (2014). “Unmanned underwater vehicles in Arctic
 764 operations,” in *22nd IAHR International Symposium on Ice*.
- 765 Paull, L., Saeedi, S., Seto, M., and Li, H. (2014). *AUV navigation and*
 766 *localization: A review*, **39**, pp. 131–149, <http://files/127/Paulletal.-2014-AUVnavigationandlocalizationAreview.pdf>.
- 767
- 768 Plueddemann, A. J., Kukulya, A. L., Stokey, R., and Freitag, L. (2012). “Autonomous
 769 Underwater Vehicle Operations Beneath Coastal Sea Ice,” IEEE/ASME Transactions
 770 on Mechatronics **17**(1), 54–64, doi: [10.1109/TMECH.2011.2174798](https://doi.org/10.1109/TMECH.2011.2174798) conference Name:
 771 IEEE/ASME Transactions on Mechatronics.
- 772 Porter, M. B. (2011). “The BELLHOP Manual and User’s Guide,” HLS Research, , 2010
 773 1–57, <http://oalib.hlsresearch.com/Rays/HLS-2010-1.pdf>.
- 774 Poulsen, A. J., and Schmidt, H. (2017). “Acoustic noise properties in the rapidly changing
 775 Arctic Ocean,” **070005**(2016), 070005, doi: [10.1121/2.0000552](https://doi.org/10.1121/2.0000552).
- 776 Randeni, S., Schneider, T., and Schmidt, H. (2020). “Construction of a
 777 high-resolution under-ice AUV navigation framework using a multidisci-
 778 plinary virtual environment,” in *2020 IEEE/OES Autonomous Underwater
 779 Vehicles Symposium, AUV 2020*, pp. 1–7, <http://files/689/Randenietal.-2020-Constructionofahigh-resolutionunder-iceAUVna.pdf>, doi:
 780 [10.1109/AUV50043.2020.9267950](https://doi.org/10.1109/AUV50043.2020.9267950).
- 781
- 782 Randeni, S., Schneider, T., Schmidt, H., Bhatt, E., and Viquez, O. (2021). “A high-
 783 resolution AUV navigation framework with integrated communication and tracking for
 784 under-ice deployments,” Field Robotics (in review).

- 785 Rossby, T., Dorson, D., and Fontaine, J. (1986). “The RAFOS System,” Journal of Atmo-
 786 spheric and Oceanic Technology **3**, 148–162.
- 787 Rypkema, N. R., Fischell, E. M., and Schmidt, H. (2017). “One-Way Travel-Time Inverted
 788 Ultra-Short Baseline Localization for Low-Cost Autonomous Underwater Vehicles,” in *2017*
 789 *IEEE International Conference on Robotics and Automation (ICRA)*, Singapore, pp. 4920–
 790 4926.
- 791 Schmidt, H., and Schneider, T. (2016). “Acoustic communication and navigation in
 792 the new Arctic-A model case for environmental adaptation,” 3rd Underwater Com-
 793 munications and Networking Conference, Ucomms 2016 <http://files/583/Schmidt,Schneider-2016-AcousticCommunicationandNavigationintheNewArctic-AModelCaseforEnvironment.pdf>, doi: [10.1109/UComms.2016.7583469](https://doi.org/10.1109/UComms.2016.7583469).
- 794
- 795 Schneider, T., Petillo, S., Schmidt, H., and Murphy, C. (2015). “The dynamic compact
 796 control language version 3,” in *OCEANS 2015-Genova*, IEEE, pp. 1–7.
- 797
- 798 Schneider, T., and Schmidt, H. (2010). “Unified command and control for heterogeneous
 799 marine sensing networks,” Journal of Field Robotics **27**(6), 876–889.
- 800 Schneider, T., and Schmidt, H. (2018). “NETSIM: A realtime virtual ocean hardware-
 801 in-the-loop acoustic modem network simulator,” in *2018 4th Underwater Communi-*

802 *cations and Networking Conference, UComms 2018*, pp. 1–5, <http://files/1047/SchneiderandSchmidt-2018-NETSIMARealtimeVirtualOceanHardware-in-the-l.pdf>,

803

804 [pdfhttp://files/1048/8493188.html](http://files/1048/8493188.html), doi: [10.1109/UComms.2018.8493188](https://doi.org/10.1109/UComms.2018.8493188).

805 Schneider, T., Schmidt, H., and Randeni, S. (2020). “Self-Adapting Under-Ice Inte-
 806 grated Communications and Navigation Network,” 2020 5th Underwater Communica-

- 807 tions and Networking Conference, UComms 2020 5, <http://files/607/Schneideretal.-Self-AdaptingUnder-IceIntegratedCommunications.pdf>.
- 808
- 809 Singh, S., Grand, M., Bingham, B., Eustice, R., Singh, H., and Freitag, L. (2006).
- 810 “Underwater acoustic navigation with the WHOI Micro-Modem,” in *Oceans 2006*,
- 811 IEEE, pp. 1–4, <http://ieeexplore.ieee.org/document/4099008/><http://files/774/Singhetal.-2006-UnderwaterAcousticNavigationwiththeWHOIMicro.pdf>, doi: 10.
- 812
- 813 [10.1109/OCEANS.2006.306853](https://doi.org/10.1109/OCEANS.2006.306853).
- 814 Timmermans, M.-L., and Winsor, P. (2013). “Scales of horizontal density structure in the
- 815 chukchi sea surface layer,” *Continental Shelf Research* **52**, 39–45.
- 816 Toole, J. M., Krishfield, R. A., Timmermans, M. L., and Proshutinsky, A. (2011). “The
- 817 Ice-Tethered profiler: Argo of the Arctic,” *Oceanography* **24**(3), 126–135, doi: [10.5670/oceanog.2011.64](https://doi.org/10.5670/oceanog.2011.64).
- 818
- 819 Uffelen, L. J. V., Howe, B. M., Nosal, E.-M., Carter, G. S., Worcester, P. F., and Dzieci-
- 820 uch, M. A. (2016). “Localization and subsurface position error estimation of gliders using
- 821 broadband acoustic signals at long range,” *IEEE Journal of Oceanic Engineering* **41**(3),
- 822 501–508.
- 823 Van Uffelen, L. J. (2021). “Global Positioning Systems: Over Land and Under Sea,” *Acous-*
- 824 *tics Today* **17**(1), 52, doi: [10.1121/at.2021.17.1.52](https://doi.org/10.1121/at.2021.17.1.52).
- 825 Van Uffelen, L. J., Nosal, E.-M., Howe, B. M., Carter, G. S., Worcester, P. F., Dzieciuch,
- 826 M. A., Heaney, K. D., Campbell, R. L., and Cross, P. S. (2013). “Estimating uncertainty
- 827 in subsurface glider position using transmissions from fixed acoustic tomography sources,”
- 828 *The Journal of the Acoustical Society of America* **134**(4), 3260–3271, doi: [10.1121/1](https://doi.org/10.1121/1).

829 4818841.

830 Webster, S. E., Eustice, R. M., Singh, H., and Whitcomb, L. L. (2009). “Prelim-
 831 inary deep water results in single-beacon one-way-travel-time acoustic navigation
 832 for underwater vehicles,” 2009 IEEE/RSJ International Conference on Intelligent
 833 Robots and Systems, IROS 2009 2053–2060, <http://files/416/Websteretal.-2009-Preliminarydeepwaterresultsinsingle-beaconone-way-travel-timeacousticnavigation.pdf>, doi: [10.1109/IROS.2009.5354457](https://doi.org/10.1109/IROS.2009.5354457).

836 Webster, S. E., Eustice, R. M., Singh, H., and Whitcomb, L. L. (2012). “Advances in
 837 single-beacon one-way-travel-time acoustic navigation for underwater vehicles,” Interna-
 838 tional Journal of Robotics Research **31**(8), 935–950, doi: [10.1177/0278364912446166](https://doi.org/10.1177/0278364912446166).

839 Webster, S. E., Freitag, L. E., Lee, C. M., and Gobat, J. I. (2015). “Towards real-time
 840 under-ice acoustic navigation at mesoscale ranges,” in *Proceedings - IEEE International
 841 Conference on Robotics and Automation*, June, IEEE, pp. 537–544, <http://files/625/Websteretal.-2015-Towardsreal-timeunder-iceacousticnavigationat.pdf>
 842 <http://files/641/Websteretal.-2015-Towardsreal-timeunder-iceacousticnavigationat.pdf>
 843 <http://files/835/Websteretal.-2015-Towardsreal-timeunde>, doi: [10.1109/ICRA.2015.7139231](https://doi.org/10.1109/ICRA.2015.7139231).

846 Wu, M., Barmin, M. P., Andrew, R. K., Weichman, P. B., White, A. W., Lively, E. M.,
 847 Dzieciuch, M. A., Mercer, J. A., Worcester, P. F., and Ritzwoller, M. H. (2019).
 848 “Deep water acoustic range estimation based on an ocean general circulation model:
 849 Application to PhilSea10 data,” The Journal of the Acoustical Society of America
 850 **146**(6), 4754–4773, <https://asa.scitation.org/doi/10.1121/1.5138606>

851 [files/947/Wuetal.-2019-Deepwateracousticrangeestimationbasedonano.pdf](#)
852 [http://files/948/1.html](#), doi: [10.1121/1.5138606](#).